Identification of Metal-Binding Residues in the *Klebsiella aerogenes* Urease Nickel Metallochaperone, UreE†

Gerard J. Colpas,‡ Timothy G. Brayman,‡ Li-June Ming,§ and Robert P. Hausinger*,‡

Departments of Microbiology and Biochemistry, Michigan State University, East Lansing, Michigan 48824-1101, and Department of Chemistry and Institute for Biomolecular Science, University of South Florida, Tampa, Florida 33620-5260

Received October 13, 1998; Revised Manuscript Received January 13, 1999

ABSTRACT: The urease accessory protein encoded by *ureE* from *Klebsiella aerogenes* is proposed to bind intracellular Ni(II) for transfer to urease apoprotein. While native UreE possesses a histidine-rich region at its carboxyl terminus that binds several equivalents of Ni, the Ni-binding sites associated with urease activation are internal to the protein as shown by studies involving truncated H144*UreE [Brayman and Hausinger (1996) *J. Bacteriol.* 178, 5410−5416]. Nine potential Ni-binding residues (five His, two Cys, one Asp, and one Tyr) within H144*UreE were independently substituted by mutagenesis to determine their roles in metal binding and urease activation. In vivo effects of these substitutions on urease activity were measured in *Escherichia coli* strains containing the *K. aerogenes* urease gene cluster with the mutated *ureE* genes. Several mutational changes led to reductions in specific activity, with substitution of His96 producing urease activity below the level obtained from a *ureE* deletion mutant. The metal-binding properties of purified variant UreE proteins were characterized by a combination of equilibrium dialysis and UV/visible, EPR, and hyperfine-shifted ^{1}H NMR spectroscopic methods. Ni binding was unaffected for most H144*UreE variants, but mutant proteins substituted at His110 or His112 exhibited greatly reduced affinity for Ni and bound one, rather than two, metal ions per dimer. Cys79 was identified as the Cu ligand responsible for the previously observed charge-transfer transition at 370 nm, and His112 also was shown to be associated with this chromophoric site. NMR spectroscopy provided clear evidence that His96 and His110 serve as ligands to Ni or Co. The results from these and other studies, in combination with prior spectroscopic findings for metal-substituted UreE [Colpas et al. (1998) *J. Biol. Inorg. Chem.* 3, 150−160], allow us to propose that the homodimeric protein possesses two nonidentical metal-binding sites, each symmetrically located at the dimer interface. The first equivalent of added Ni or Co binds via His96 and His112 residues from each subunit of the dimer, and two other N or O donors. Asp111 either functions as a ligand or may affect this site by secondary interactions. The second equivalent of Ni or Co binds via the symmetric pair of His110 residues as well as four other N or O donors. In contrast, the first equivalent of Cu binds via the His110 pair and two other N/O donors, while the second equivalent of Cu binds via the His112 pair and at least one Cys79 residue. UreE sequence comparisons among urease-containing microorganisms reveal that residues His96 and Asp111, associated with the first site of Ni binding, are highly conserved, while the other targeted residues are missing in many cases. Our data are most compatible with one Ni-binding site per dimer being critical for UreE's function as a metallochaperone.

Metallochaperones are intracellular metal-binding proteins that protect the cell from reactivity of free metal ions while delivering specific cations to target metalloproteins. Perhaps the best characterized metallochaperones are those involved in cellular trafficking of copper (*1*). For example, yeast uses the Ctr1 protein to transport Cu(I) across the plasma membrane and then transfers the metal ion to one of at least three small, soluble, Cu chaperone proteins (Atx1, Lys7, and Cox17) that deliver the metal ion to distinct sites (*2*−*4*). The precise mechanisms for Cu delivery by these Cu-binding proteins are poorly defined, and auxiliary proteins may be required for loading of the metal ion into these metallochaperones or for achieving proper target specificity. Numerous other enzymes are known to require accessory proteins for metallocenter assembly [reviewed in (*5*)], and it is likely that metallochaperones participate in specific delivery of many of the essential transition metals to a variety of additional apoproteins.

Nickel is specifically incorporated into five enzymes (hydrogenase, carbon monoxide dehydrogenase/acetyl-*S*-coenzyme A synthase, methyl-*S*-coenzyme M reductase, one form of superoxide dismutase, and urease) [reviewed in (*6*)], and several distinct Ni-specific metallochaperone proteins appear to exist. For example, HypB is essential for Ni insertion into hydrogenase by a process that requires GTP hydrolysis (*7*, *8*). The amino-terminal region of HypB in some, but not all, microorganisms contains a histidine-rich region that has been shown to bind Ni (*9*, *10*). Experimental evidence obtained with cells synthesizing mutant protein lacking the His-rich region is consistent with HypB serving both in Ni

† This work was supported by NIH Grant DK 45686 to R.P.H.

* To whom correspondence should be addressed at 160 Giltner Hall. Phone: (517) 353-9675. Fax: (517) 353-8957. E-mail: Hausinge@pilot.msu.edu.

‡ Michigan State University.

§ University of South Florida.

10.1021/bi982435t CCC: $18.00
Published on Web 03/11/1999

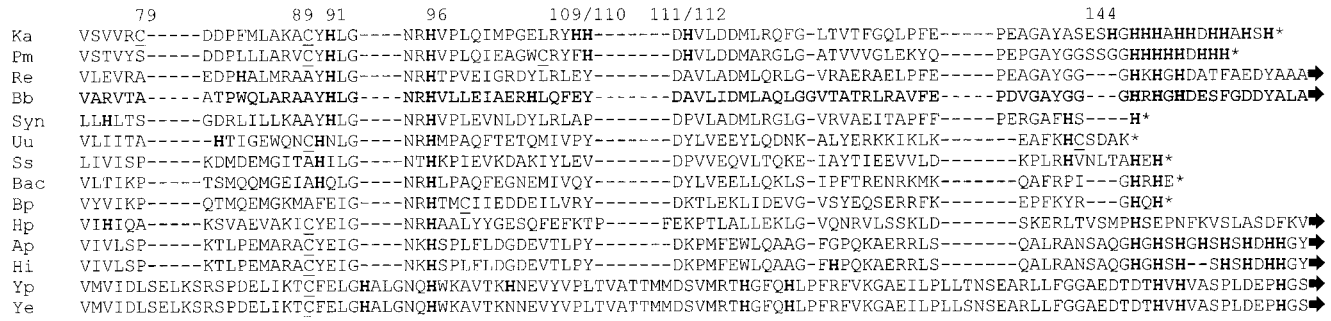

FIGURE 1: UreE sequence comparisons. The carboxyl-terminal region (residues 74 through 158) of *Klebsiella aerogenes* UreE [Ka, (*19*)] is compared to the homologous UreE regions from *Proteus mirabilis* [Pm, (*31*)], *Ralstonia eutropha* (Re, Genbank accession no. Y13732), *Bordetella bronchiseptica* [Bb, (*32*)], *Synechocystis* sp. strain PCC6803 [Syn, (*33*)], *Ureaplasma urealyticum* [Uu, (*34*)], *Streptococcus salivarius* [Ss, (*35*)], *Bacillus* sp. TB-90 [Bac, (*36*)], *Bacillus pasteurii* [Bp, (*37*)], *Helicobacter pylori* [Hp, (*38*)], *Actinobacillus pleuropneumoniae* [Ap, (*39*)], *Haemophilus influenzae* [Hi, (*40*)], *Yersinia pseudotuberculosis* [Yp, (*41*)], and *Yersinia enterocolitica* [Ye, (*42*)]. Termination signals are indicated by an asterisk, and an arrow is shown for those sequences which continue beyond the region indicated. All cysteine residues are underlined, and both of those present in *K. aerogenes* UreE were targeted for mutagenesis. Similarly, histidine residues are shown in boldface type, and all five that are present in H144*UreE were subjected to mutagenesis. Two additional residues that were changed included tyrosine within the CYH motif at position 90 and aspartate found in the HHDH motif at position 111.

delivery to hydrogenase as well as in Ni storage (*11*). Activation of CO dehydrogenase similarly involves a protein containing a His-rich region, CooJ, where in this case the potential metal-binding motif is located at the carboxyl terminus (*12*). Analogous to the case of *hypB* mutants (*13*), *cooJ* mutants can be phenotypically suppressed by increasing the Ni concentration in the medium (*12*). Purified CooJ from *Rhodospirillum rubrum* has been shown to bind four Ni per monomer, and to competitively bind several other divalent metals (*14*). In addition, an interaction with several other proteins, including CO dehydrogenase, was observed during purification of this protein. Extensive studies have revealed many aspects of the elaborate metallocenter assembly pathway for synthesis of the Ni-containing coenzyme F_{430} found in methyl-*S*-coenzyme M reductase (*15*), but it remains unclear whether a metallochaperone participates in this process. Similarly, no evidence has been reported that a chaperone aids in synthesis of Ni-containing superoxide dismutase (*16*). The work described in this paper focuses on characterization of a possible Ni metallochaperone associated with urease. As detailed below, the UreE accessory protein, shown to be associated with urease activation (*17*), is a Ni-binding protein (*18*).

Purified *Klebsiella aerogenes* UreE reversibly binds 5−6 Ni(II) ions per 34 kDa homodimer (average K_d ~10 μM) (*18*). Spectroscopic experiments with this protein indicate the presence of pseudo-octahedral Ni(II) coordinated by an average of 3−5 imidazole ligands, implicating a role for the carboxyl terminus where 10 of the last 15 residues are histidine (*19*). Despite its distinctive sequence, however, the His-rich region found in the *K. aerogenes* protein is not conserved in all UreE homologues (Figure 1). Furthermore, a truncated form of *K. aerogenes* UreE lacking the His-rich region, termed H144*UreE,[1] is competent for activating urease in vivo (*20*). Thus, internal Ni-binding sites, not the histidine residues at the carboxyl terminus, are necessary for UreE to assist in *K. aerogenes* urease activation. Equilibrium dialysis measurements with H144*UreE indicate that two Ni(II) per dimer are cooperatively bound, with an average K_d of ~8 μM. Competition experiments with Cu, Zn, Co, and Cd indicate that these divalent metal ions compete (to varying degrees) with Ni binding to H144*UreE in vitro (*20*). Spectroscopic studies of Ni, Cu, and Co binding to H144*UreE reveal the two binding sites per homodimer to be distinct in their properties, consistent with an observed sequential binding pattern for the two sites (*21*). In addition, the coordination environments differ for each type of metal. Thus, the two Cu sites have tetragonal coordination environments with two histidine donors each, but a cysteine donor coordinates only the second metal ion that is bound to the dimer. Co is bound exclusively by N/O donors including at least three histidines in the two pseudo-octahedral sites. Ni is chelated in a manner similar, but not identical, to Co with at least three histidines in two approximately six-coordinate N/O sites. The differences in coordination environments observed for each type of metal ion are proposed to facilitate in vivo Ni selection for urease activation (*21*).

Here, we have used site-directed mutagenesis methods to create variants of H144*UreE in order to identify the metal-binding ligands. The variants include substitution of alanine for each of two cysteine residues (positions 79 and 89) and all five histidines (residues 91, 96, 109, 110, and 112) in the truncated protein (Figure 1). In addition, the tyrosine at position 90 (associated with a CYH motif) and an aspartate at position 111 (in a HHDH motif) were changed to phenylalanine and alanine, respectively. We examined the effects of these nine changes on the ability of the metallochaperone to form active urease in vivo, and we characterized the interactions between purified H144*UreE variants and selected metal ions by equilibrium dialysis and spectroscopic methods. Based on results from these studies, in combination with those from prior spectroscopic analyses (*21*), we propose a model in which two distinct metal-binding sites are present at the dimer interface, and we identify several ligands at each metal-binding site. Furthermore, we show that one of the metal sites (involving the highly conserved His96 and Asp111 residues) appears to be more important for in vivo activation of urease than the second site.

[1] Abbreviations: H144*UreE, product derived from the *ureE* gene containing a stop codon at the position corresponding to His144; EDTA, ethylenediaminetetraacetic acid; EPR, electron paramagnetic resonance; NMR, nuclear magnetic resonance; NTA, nitrilotriacetic acid; PAGE, polyacrylamide gel electrophoresis; PEB, 20 mM phosphate buffer containing 0.5 mM EDTA and 1 mM β-mercaptoethanol; SDS, sodium dodecyl sulfate; XAS, X-ray absorption spectroscopy.

Table 1: Primers Used in This Work

plasmid generated	primers[a]
pTBEFC79A (+*Bss*HII)	GTAGT*GCGC**GC**C*GACGATCC
pTBEFC89AH144* (−*Stu*I)	GCGA*AGGCC**GC**C*TACCACCTC
pTBEFY90FH144* (−*Stu*I)	CTGGCGAA*GGC**GT**C*T**T**CCACCTCGGCAAC
pTBEFH91AH144* (−*Stu*I)	GCGA*AGGC**GT**C*TACG**C**C*CTCGGCAACC
pTBEFH96AH144*	GCAACCGT**GC**CGTGCCGCTG
pTBEFH109AH144*	GCGAGCTGCTAC**GC**TCACGATCACGTGC
pTBEFH110AH144*	GCTGCGCTACCAT**GC**CGATCACGTGCTG
pTBEFD111AH144*	CGCTACCATCACG**C**TCACGTGCTGGAC
pTBEFH112AH144*	GCTACCATCACGAT**GC**CGTGCTGGACGATATGC
pUC19 (−*Hin*dIII)	CAGGCATGC*A**C**GC**GT**C*GGCGTAATC

[a] Bases encoding the target amino acid are underlined. Locations of restriction sites are italicized. Changes in the sequence are shown in boldface type. The reverse primer (when used) covered the same sequence.

EXPERIMENTAL PROCEDURES

Site-Directed Mutagenesis and Plasmid Construction. Unless otherwise indicated, all restriction digestions and common DNA manipulations were performed by using standard procedures (*22*). Primers (Table 1) were synthesized at the Michigan State University Macromolecular Structure and Sequencing Facility and phosphorylated with T4 kinase (Gibco BRL). Site-directed mutagenesis was accomplished by using the Transformer kit (Clontech) or the Quikchange kit (Stratagene). The Transformer kit required, in addition to the *ureE* mutagenic oligonucleotides, an oligonucleotide used to mutate a *Hin*dIII site to facilitate selection. The C89A, Y90F, and H91A *ureE* mutagenic oligonucleotides were designed to incorporate the desired mutation as well as to eliminate a unique *Stu*I site, facilitating the identification of mutant plasmids by restriction digestion analysis. Similarly, the C79A mutagenic oligonucleotide introduced a new *Bss*HII site. Plasmids from recombinant colonies were isolated by using the Wizard MiniPrep DNA purification system (Promega, Madison, WI) and screened by restriction digestion analysis. All mutants were sequenced throughout the entire open reading frame of *ureE*. DNA sequencing was performed by the Michigan State University/U.S. Department of Energy−Plant Biology Laboratory using dye termination chemistry and an Applied Biosystems automated DNA sequencer.

Plasmids used in this study are listed in Table 2. The *K. aerogenes* urease gene cluster (*ureDABCEFG*) cloned into pUC8 is denoted pKAU17 (*23*). The pKAU17x derivative of this plasmid had the vector *Aat*II site eliminated by partial digestion with *Aat*II, treatment with Klenow fragment to produce blunt ends, reannealing with T4 DNA ligase, and selection based on restriction pattern (*24*). Similarly, pKAU17-H144* lacked the vector *Aat*II site and additionally possessed a stop codon in *ureE* at the position encoding His144 to produce a 15-residue truncated UreE termed H144*UreE (*20*). Additional plasmids that were used in control experiments included pKK17Δ*ureE-1*, pKK17, and pKK17H144*. The first of these controls was derived from pKAU17 containing a deletion in *ureE* (*17*), after transferring the 5.5 kbp *Eco*RI/*Hin*dIII fragment into pKK223-3. The pKK17 and pKK17-H144* plasmids were derived by inserting the 5.5 kbp *Eco*RI/*Hin*dIII fragment containing the intact urease gene cluster (from pKAU17) or the cluster containing a truncated *ureE* (from pKAU17H144*) into similarly digested pKK223-3.

Three strategies were used to generate clones encoding the nine variant forms of truncated H144*UreE either within the context of the other urease genes (on pKAU17x and the pKK223-3 cloning and expression vector) or separately (on the pET21 cloning and expression vector). The first approach, used for the C79A variant, involved mutagenesis of full-length *ureE* carried by pTBEF (*20*) to yield pTBEFC79A. The *ureE*-containing *Bam*HI−*Aat*II fragment of pTBEFC79A was cloned into the corresponding region of pKAU17x to yield pKAU17C79A. The *Bam*HI−*Hin*dIII fragment of this plasmid (encoding C79AUreE as well as UreF and UreG) was cloned into pET21 to yield pETC79A. In addition, pETH144* (*20*) was digested with *Avr*II and *Hin*dIII to remove *ureG*, and the 7.1-kbp fragment was treated with Klenow fragment of *E. coli* DNA polymerase and reannealed with T4 DNA ligase to produce pETH144*Δ*ureG*. Finally, the *Bam*HI−*Stu*I fragment (containing the C79A-associated region in *ureE*) of pETC79A was ligated to similarly digested pETH144*Δ*ureG* (containing the stop codon within *ureE*) to yield pETC79AH144* which encodes C79A/H144*UreE. The *ureE*-containing *Bam*HI−*Aat*II fragment of pETC79A-H144* was cloned into the corresponding region of pKAU17x to yield pKAU17C79AH144*. The second strategy for mutagenesis, used for the H96A variant, involved mutagenesis of *ureE* within pTBEFH144* (*20*) to yield plasmid pTBEFH96AH144*. The *ureE*-containing *Bam*HI−*Aat*II fragment of pTBEFH96AH144* was cloned into the corresponding region of pKAU17x to yield pKAU17H96AH144*. The *Bam*HI−*Hin*dIII fragment of this plasmid was ligated to similarly digested pET21 to yield pETH96AH144*. The third strategy, used to obtain the C89A, Y90F, H91A, H109A, H110A, D111A, and H112A variants of H144*UreE, also involved mutagenesis of pTBEFH144*. The *Bam*HI−*Hin*dIII fragments of mutated pTBEFH144* plasmids were ligated to similarly digested pET21 to provide pETC89A-H144* and the six analogous plasmids. Similarly, the 1.1-kbp *Bam*HI−*Aat*II fragments of mutated pTBEFH144* plasmids were cloned into the corresponding region of pKAU17x to yield the other seven pKAU17H144* variants. Finally, the *Eco*RI−*Hin*dIII fragment of pKAU17C79AH144* and the eight analogous plasmids were cloned into similarly digested pKK223-3 to give the pKK17H144* variants.

Bacterial Strains and Growth Conditions. E. coli DH5α cells were used for routine recombinant DNA work. Cells were grown overnight at 37 °C in LB liquid or agar medium containing 100 $\mu g \cdot mL^{-1}$ ampicillin. For DNA purification, cells were grown in MR2001 growth media (MacConnell Research, San Diego, CA). Studies involving site-directed mutagenesis made use of *E. coli* BMH 71-18 *mutS* cells

Table 2: Plasmids Used

plasmid	characteristics	reference
pKAU17	*K. aerogenes ureDABCEFG* genes cloned into pUC8	(*23*)
pKAU17x	pKAU17 with elimination of vector *Aat*II site	(*24*)
pKAU17H144*	pKAU17x with *ureE* mutated to encode His144*UreE	(*20*)
pKAU17C79A	pKAU17x with *ureE* mutated to encode C79A UreE	this study
pKAU17C79AH144*, pKAU17C89AH144*, pKAU17Y90FH144*, pKAU17H91AH144*, pKAU17H96AH144*, pKAU17H109AH144*, pKAU17H110AH144*, pKAU17D111AH144*, pKAU17H112AH144*	pKAU17x with *ureE* mutated to encode C79A, C89A, Y90F, H91A, H96A, H109A, H110A, D111A, and H112A derivatives of H144*UreE	this study
pKAU17Δ*ureE*−*1*	pKAU17 containing a deletion within *ureE*	(*17*)
pTBEF	*Bam*HI−*Avr*II fragment of pKAU17 (containing *ureEF*) cloned into *Bam*HI- and *Xba*I-digested pUC19	(*20*)
pTBEFC79A	pTBEF with *ureE* mutated to encode C79A variant of UreE	this study
pTBEFH144*	pTBEF with *ureE* mutated to encode H144*UreE	(*20*)
pTBEFC89AH144*, pTBEFY90FH144*, pTBEFH91AH144*, pTBEFH96AH144*, pTBEFH109AH144*, pTBEFH110AH144*, pTBEFD111AH144*, pTBEFH112AH144*	pTBEFH144* mutated to encode C89A, Y90F, H91A, H96A, H109A, H110A, D111A, and H112A variants of H144*UreE	this study
pKK223-3	cloning and expression vector	Pharmacia
pKK17	*K. aerogenes ureDABCEFG* genes on an *Eco*RI−*Hin*dIII fragment cloned into pKK223-3	this study
pKK17H144*	pKK17 with *ureE* mutated to encode His144*UreE	this study
pKK17C79AH144*, pKK17C89AH144*, pKK17Y90FH144*, pKK17H91AH144*, pKK17H96AH144*, pKK17H109AH144*, pKK17H110AH144*, pKK17D111AH144*, pKK17H112AH144*	pKK17H144* with *ureE* mutated to encode C79A, C89A, Y90F, H91A, H96A, H109A, H110A, D111A, and H112A derivatives of H144*UreE	this study
pKK17Δ*ureE*−*1*	pKK17 containing deletion within *ureE*	this study
pET21	cloning and expression vector	Promega
pETC79A	*Bam*HI−*Hin*dIII fragment of pKAU17C79A (encoding full-length C79A variant of UreE and containing *ureFG*) cloned into pET21	this study
pETH144*	*Bam*HI−*Hin*dIII fragment of pKAU17H144* (encoding H144*UreE and containing *ureFG*) cloned into pET21	(*20*)
pETH144*Δ*ureG*	pETH144* with *ureG* deleted (encodes H144*UreE and UreF)	this study
pETC79AH144*	pETH144* Δ*ureG* with site mutated to encode C79A	this study
pETH96AH144*	*Bam*HI−*Hin*dIII fragment of pKAU17H96AH144* ligated to similarly digested pET21 to encode H96A variant of H144*UreE	this study
pETC89AH144*, pETY90FH144*, pETH91AH144*, pETH109AH144*, pETH110AH144*, pETD111AH144*, pETH112AH144*	*Bam*HI-*Hin*dIII fragments of pTBEFH144* mutants encoding C89A, Y90F, H91A, H109A, H110A, D111A, and H112A variants of H144*UreE ligated to similarly digested pET21	this study

(Clontech, Palo Alto, CA) or *E. coli* XL1-Blue cells (Stratagene) carrying the indicated plasmids. *E. coli* HMS174-(DE3) or *E. coli* BL21(DE3) cells (Novagen, Madison, WI) carrying derivatives of pET21 were used for overproduction of recombinant UreE. These cultures were grown in TB medium (*22*) containing 100 $\mu g \cdot mL^{-1}$ ampicillin to OD_{600} ~1, induced with 1 mM isopropyl β-D-thiogalactopyranoside (IPTG, Sigma, St. Louis, MO), and harvested after 4−6 h.

In Vivo Studies. *E. coli* HMS174(DE3) cells containing variants of pKK17H144* were grown for approximately 24 h in 50 mL of LB medium supplemented with 100 $\mu g \cdot mL^{-1}$ ampicillin, 1 mM IPTG, and variable $NiCl_2$ concentrations. Cells were harvested by centrifugation, resuspended in 2.5 mL of 20 mM phosphate buffer containing 0.5 mM EDTA and 1 mM β-mercaptoethanol (PEB) at pH 7.4, and twice disrupted in a French pressure cell (18 000 $lb \cdot in^{-2}$) to give cell extracts for the urease activity measurements.

Assays. Urease activity was measured by quantifying the rate of ammonia release from urea by formation of indophenol, which was measured at 625 nm (*25*). Assay buffer contained 25 mM HEPES (pH 7.75), 50 mM urea, and 0.5 mM EDTA. One unit of activity was defined as the amount of enzyme required to hydrolyze 1 μmol of urea per minute at 37 °C. Protein concentrations were determined according to Lowry et al. (*26*) or by using a commercial protein assay (Bio-Rad, Hercules, CA) with bovine serum albumin as the standard.

Purification of UreE Variants. Variants of H144*UreE protein generally were purified by using a modification of the method described previously for H144*UreE (*20*). Cultures (2−3 L) of *E. coli* HMS174(DE3) or BL21(DE3) containing pET21-derived plasmids encoding the H144*UreE variants were harvested by centrifugation, resuspended in 20 mM Tris-HCl (pH 7.9) containing 500 mM NaCl and 60 mM imidazole (buffer A) with 0.5 mM phenylmethylsulfonyl fluoride, and disrupted by two passages through a French pressure cell at 18 000 $lb \cdot in^{-2}$. Cell debris was removed by centrifugation at 100000*g* for 40 min at 4 °C. A nitrilotriacetic acid (NTA) column (Qiagen, Chatsworth, CA) was charged with 50 mM $NiSO_4$ and equilibrated with buffer A. Cell extracts were loaded onto the column, and buffer A was used to wash the resin until the A_{280} reached base line. Bound proteins were eluted in 20 mM Tris-HCl (pH 7.9), 500 mM NaCl, and 1 M imidazole. Fractions were analyzed by gel electrophoresis (see below), and samples of interest were pooled, treated with 1 mM EDTA to eliminate contaminating

metals, concentrated by using an Amicon-50 stirring concentrator (Amicon, Beverly, MA), and dialyzed overnight twice in 20 mM Tris-HCl (pH 7.5) containing 100 mM NaCl.

For the H110A and H112A H144*UreE variants, an alternative purification protocol was required because these proteins did not bind to the Ni−NTA column. Cells were resuspended in PEB (pH 7.4) buffer and disrupted as described above. The resulting cell extracts were applied to a DEAE-Sepharose column equilibrated with the same buffer and eluted with a linear gradient from 0 to 0.5 M KCl in PEB, pH 7.4, buffer. The H144*UreE variants eluted from the resin at approximately 0.3 M salt. The pooled samples were dialyzed, applied to a Mono-Q column (Pharmacia) equilibrated in PEB (pH 6.8) buffer, and eluted with a linear salt gradient to 0.5 M NaCl in this buffer, giving nearly homogeneous H144*UreE variants. Further purification was achieved by gel filtration chromatography using a Superose-12 column (Pharmacia) equilibrated with PEB (pH 7.4) buffer. The protein was analyzed, concentrated, and dialyzed as described above for the other variants.

Polyacrylamide Gel Electrophoresis (PAGE). All gel electrophoresis was carried out by using denaturing buffers as described by Laemmli (*27*) and a 12% polyacrylamide resolving gel with a 4.5% polyacrylamide stacking gel. Samples were denatured at 100 °C for 5 min in buffers containing 3% sodium dodecyl sulfate (SDS) and 5% β-mercaptoethanol. Gels were stained with Coomassie brilliant blue.

Equilibrium Dialysis. Protein samples of H144*UreE variants (5 μM peptide in 0.5 mL) were dialyzed against 0.5 mL of buffer containing $^{63}NiCl_2$ (1,445 mCi/mmol; Du Pont NEN Research Products, Inc., Wilmington, DE) and various concentrations of unlabeled $NiCl_2$ using an equilibrium microvolume dialyzer (Hoeffer Scientific Products, San Francisco, CA) equipped with precut dialysis membranes (MW cutoff 12 000−14 000). The buffer used was 20 mM Tris-HCl (pH 7.5) containing 100 mM NaCl. After overnight equilibration at room temperature, an aliquot from each compartment was measured for radioactivity by using a Beckman LS7000 liquid scintillation system and Safety Solve scintillation fluid (Research Products International Corp., Mount Prospect, IL). Data were fitted by the method of least squares to a modification of the Adair equation (*28*) for fractional saturation (Y):

$$Y = \frac{N[\mathrm{Ni}]\{1/K_1 + ([\mathrm{Ni}]/K_1K_2)\}}{[1 + (2[\mathrm{Ni}]/K_1) + ([\mathrm{Ni}]^2/K_1K_2)]}$$

where K_1 and K_2 are dissociation constants for binding the first and second Ni ions, and N is the number of Ni ions bound per dimer. A measure of cooperativity was determined graphically for each sample using a Hill plot (*28*) based on data points found between 0.2 and 1.8 Ni/dimer. The Hill coefficients were obtained from the slope of a linear fit to the data, and the average dissociation constant [$K_{d(avg)}$ value] was determined from the intercept.

Spectroscopy. Electronic absorption spectra of H144*UreE variants (200 μM dimer) in the presence of increasing equivalents of Cu ions were recorded and analyzed on a DU-7500 UV−visible spectrophotometer (Beckman, Fullerton, CA) using a 150 μL cuvette and 20 mM Tris-HCl buffer (pH 7.5) containing 100 mM NaCl. Titrations with Ni ions were also carried out with a subset of the samples using 200 or 500 μM dimer. X-band electron paramagnetic resonance (EPR) spectra were obtained on a Bruker ESP-300E spectrometer. Samples were prepared in 10 mM Tris-HCl buffer (pH 7.5) containing 50 mM NaCl and 30% glycerol to aid in glass formation. Spectra were recorded on frozen solutions at 77 K. Simulations of the base-line-corrected EPR spectra made use of the EPR/POWFIT programs (*29*). The proton nuclear magnetic resonance (NMR) spectra of the paramagnetic Ni(II) and Co(II) derivatives of selected H144*UreE variants were acquired at 298 K on a Bruker AMX360 NMR spectrometer operated at 360 MHz. Selective excitation of solvent-exchangeable signals was performed using the 1-*3*-3-*1* hard pulse sequence (*30*). The spectra for Ni-containing proteins were compared to that reported previously for H144*UreE which was obtained using a single 90° pulse with a 50 ms presaturation decoupler pulse. A Gaussian apodization function with a 5% shift and a line-broadening factor of −50 Hz was applied to the FIDs prior to Fourier transformation. Samples were prepared in 10 mM phosphate buffer (pH 7.2) with 10% D_2O added to use as a frequency lock. When spectra were acquired in samples without D_2O, the field was shimmed by monitoring the FID of the water signal.

RESULTS

In Vivo Studies. The effects of the amino acid substitutions within H144*UreE on its ability to aid in urease activation were examined by measuring urease activities in cell extracts of *E. coli* HMS174(DE3) containing derivatives of pKK17-H144*. For comparison, analogous studies were carried out with cells containing plasmid derivatives encoding the wild-type, nontruncated, UreE as well as with cells containing a *ureE* deletion. In all cases, expression levels of the urease genes were comparable based on SDS−PAGE analyses that revealed similar intensities of the bands corresponding to urease peptides. The effects on urease activity of varying the growth medium Ni ion concentration for selected strains are shown in Figure 2. The results obtained for cells containing pKK17 (encoding wild-type UreE) and pKK17-H144* (coding for H144*UreE) were similar to each other (data not shown), consistent with previous results reported for pKAU17 and pKAU17H144* (*20*), and confirm the nonimportance of the carboxyl-terminal His-rich region found in wild-type protein for urease activation. Likewise, cells containing pKK17Δ*ureE-1* (with a *ureE* deletion) possessed significantly less urease activity compared to cells containing wild-type protein, in agreement with prior work indicating that UreE facilitates urease activation, but is not essential to this process (*17*). The patterns observed for the mutants all showed increasing urease activity with increasing Ni concentration until approximately 1 mM Ni was added, after which cell growth was inhibited due to Ni toxicity. For cells containing C89A, Y90F, H91A, and H109A variants of H144*UreE, the activities were closely similar to those found for cells containing wild-type UreE or H144*UreE (data not shown). For other cultures, however, differences from this pattern were clearly observed. For example, urease activity was significantly reduced at all Ni concentrations for cells containing the H96A derivative of H144*UreE (Figure 2), and only approached the level of urease activity found for

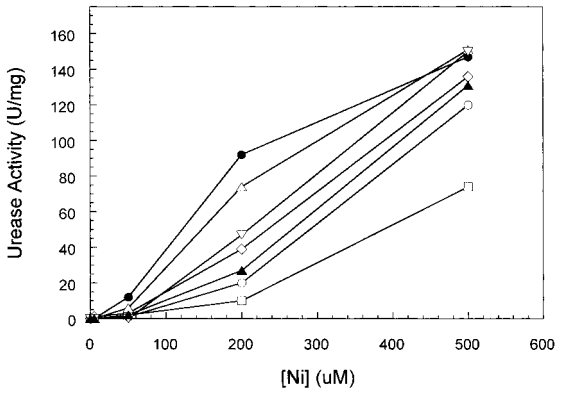

FIGURE 2: Effects of UreE modifications on in vivo urease activity. *E. coli* HMS174 (DE3) cells harboring the indicated plasmids were grown overnight in LB media with varying Ni ion concentrations. Cells were disrupted, and extracts were assayed for urease specific activity. Plasmids used (and the UreE variants they encode) include pKK17H144* (H144*UreE, ●), pKK17Δ*ureE-1* (*ureE* deleted, ▲), pKK17C79AH144* (C79A/H144*UreE, ◇), pKK17H96AH144* (H96A/H144*UreE, □), pKK17H110AH144* (H110A/H144*UreE, △), pKK17D111AH144* (D111A/H144*UreE, ○), and pKK17H-112AH144* (H112A/H144*UreE, ▽).

cells containing the *ureE* deletion plasmid at approximately 1 mM Ni (data not shown). A less dramatic, but still significant, reduction in activity was found for the cells containing the D111A/H144*UreE. The data associated with these cells tracked closely with those of the *ureE* deletion plasmid through 0.5 mM Ni. For cells containing the C79A or H112A versions of H144*UreE, reduction in urease activity was observed at 200 μM Ni compared to the control cells. Finally, cells containing H110A/H144*UreE exhibited activities that closely tracked the control plasmid, but did show a reduction in activity at 1 mM $NiCl_2$ (data not shown).

Purification. Most modified H144*UreE proteins were easily purified using Ni−NTA affinity chromatography as demonstrated by the presence of homogeneous peptides after SDS−PAGE (data not shown). This result was similar to that seen for H144*UreE purification (*20*), with yields of approximately 15−20 mg of protein per liter of culture. In contrast, two of the mutant proteins, H110A/H144*UreE and H112A/H144*UreE, did not bind to the Ni−NTA column and had to be purified by a different procedure. A combination of DEAE-Sepharose and Mono-Q chromatographies was sufficient to generate nearly homogeneous protein in each case. Further purification was achieved by gel filtration chromatography on a Superose-12 column. The resultant proteins were similar to the other variants obtained by Ni−NTA affinity chromatography in terms of purity and yield (data not shown).

Equilibrium Dialysis. The number of Ni ions bound to each of the H144*UreE derivatives and the calculated dissociation constants for binding were assessed by equilibrium dialysis experiments (Table 3). In addition, the Hill coefficients were calculated as a measure of cooperativity for the proteins which bind two Ni ions. For most of the variants studied here, the values observed were similar to those obtained for H144*UreE (Figure 3), and the values for this protein were more accurate than those previously reported (*20*) because of improved curve-fitting procedures. All variants except H110A/H144* and H112A/H144* bound approximately two Ni ions with an average K_d of 6−11 μM and retained a degree of positive cooperativity with a Hill coefficient between 1.3 and 2.1, in good agreement with the values of 8.6 μM and 1.69 obtained for H144*UreE. Consistent with the inability of the H110A and H112A variants of H144*UreE to bind to the Ni affinity column, these proteins showed reduced Ni-binding ability when measured by equilibrium dialysis methods (Figure 3). For H110A/H144*UreE, approximately 1.3 Ni were bound with a K_d of 16 μM. Likewise, H112A/H144*UreE bound approximately 1.1 Ni, but with a greatly altered K_d of 36 μM.

Electronic Spectroscopy. The H144*UreE mutant proteins were examined by UV−visible spectroscopy to probe for changes that occur in the presence of divalent Ni and Cu ions. Consistent with previous results for H144*UreE (*21*), variants which retained the ability to bind two Ni ions produced a weak d−d band at approximately 380 nm ($\epsilon \sim 75\ M^{-1}\ cm^{-1}$) that was only fully developed upon addition of 2 equiv of this metal ion to the dimer (data not shown). By contrast, the H112/H144* variant exhibited a shift in this d−d band to approximately 415 nm ($\epsilon \sim 100\ M^{-1}\ cm^{-1}$) upon addition of 1 equiv Ni ion. The spectra obtained from addition of Cu to most of the variants also were indistinguishable from the previously characterized spectra for H144*UreE (*23*) and consisted of a Cys-to-Cu charge-transfer band at 370 nm ($\epsilon \sim 2500\ M^{-1}\ cm^{-1}$), that was generated primarily upon addition of the second equivalent of metal ion to the dimer, and a broad d−d transition observed near 625 nm ($\epsilon \sim 250\ M^{-1}\ cm^{-1}$). In contrast, the spectra obtained for C79A/H144*UreE lacked a 370 nm charge-transfer band, although they retained a less intense and red-shifted long-wavelength band (data not shown). These results indicate the loss of the Cys-to-Cu charge-transfer interaction upon removal of Cys79. The 370 nm band was retained in the C89A/H144*UreE variant, but the protein solubility was diminished upon Cu binding with significant precipitation observed after addition of the second equivalent of metal ion. The addition of Cu to H112A/H144*UreE also failed to produce the 370 nm band and caused a shift of the 625 nm band to longer wavelength (∼750 nm; data not shown). For H110A/H144*UreE, the 370 nm band was observed; however, the intensity of the band was reduced in the presence of 2 Cu/dimer, compared to the H144*UreE sample, and was not enhanced with further additions of Cu.

EPR Spectroscopy. EPR spectra were obtained for the H144*UreE variants in the presence of 1 and 2 equiv of Cu and fitted with a simulation program to provide the results given in Table 4. Consistent with previous results for H144*UreE (*21*), all of the spectra were typified as tetragonal type 2 Cu sites; however, important but subtle differences were observed in some of the variants. The values obtained for the 1 Cu/dimer H144*UreE spectrum yielded $g_z = 2.28$ with $A_z = 154$ G and $g_{x/y} = 2.08/2.05$ with $A_{x/y} = 9/12$ G arising from Cu hyperfine. Superhyperfine splitting was observed in g_{xy} with ∼15 G spacing typical of ^{14}N directly bound to the Cu (Figure 4A). Addition of the second Cu per dimer resulted in the superimposition of a distinct spectrum (g-values of 2.32 with $A_z = 150$ G and 2.08/2.06 with $A_{x/y} = 6/8$ G) on the first spectrum (Figure 4B). The spectra obtained for the 1 Cu/dimer and the 2 Cu/dimer samples of C79A/H144*UreE are nearly identical to each other, but differ markedly from the above in both g and A values (Figure 4C). The spectrum obtained for H110A/H144*UreE

Table 3: Ni(II) Binding by H144*UreE Variants[a]

protein	no. of Ni/dimer[b]	K_{d1}[b] (μM)	K_{d2}[b] (μM)	Hill coefficient[c]	$K_{d(avg.)}$[c] (μM)
H144*UreE	2.01 (0.05)	47 (20)	1.5 (0.7)	1.69	8.6
C79A/H144*UreE	1.90 (0.05)	32 (19)	1.2 (0.8)	1.55	8.0
C89A/H144*UreE	2.25 (0.1)	21 (5)	4.8 (1.8)	1.46	7.4
Y90F/H144*UreE	2.06 (0.05)	70 (34)	1.8 (1.0)	1.75	8.7
H91A/H144*UreE	2.02 (0.1)	85 (37)	1.6 (0.7)	2.10	10.6
H96A/H144*UreE	1.92 (0.1)	39 (30)	3.0 (2.8)	1.68	8.3
H109A/H144*UreE	2.49 (0.1)	17 (2.8)	7 (2.5)	1.51	7.7
H110A/H144*UreE	1.33 (0.05)	16 (3)	–	–	–
D111A/H144*UreE	2.22 (0.1)	19 (4)	7 (3)	1.33	6.7
H112A/H144*UreE	1.11 (0.1)	36 (13)	–	–	–

[a] Protein concentrations were approximately 5 μM in 20 mM Tris-HCl (pH 7.5) with 100 mM NaCl. Numbers in parentheses represent the standard deviation for each value. [b] Determined from curve fits to binding data. [c] Determined from Hill plots.

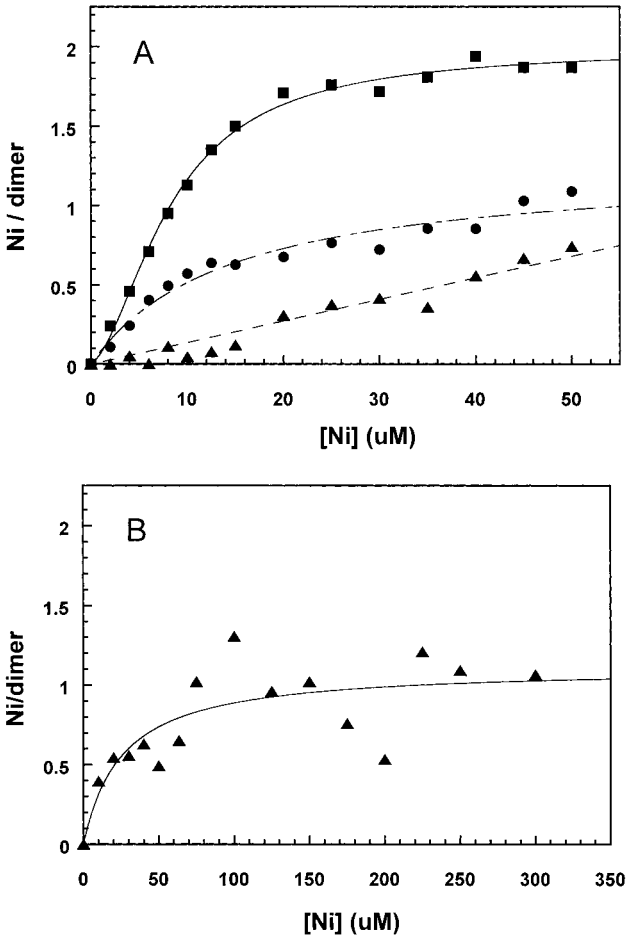

FIGURE 3: Nickel ion binding to H144*UreE variants measured by equilibrium dialysis. (A) The interaction of Ni ions with H144*UreE (■), H110A/H144*UreE (●), and H112A/H144*UreE (▲) was examined at protein concentrations of approximately 5 μM dimer in 20 mM Tris-HCl (pH 7.5) with 100 mM NaCl. (B) H112A/H144*UreE (5 μM) was examined in the same buffer over an expanded range of Ni ion concentrations.

with 1 Cu/dimer added (Figure 4D) differs from that obtained for the 1 Cu/dimer H144*UreE, but matches more closely to the features observed for the spectrum obtained from the second binding site of this protein. The H112A/H144*UreE spectrum was only able to be fitted by assuming the presence of two sites of equal intensity with large differences in g_z and A_z (Figure 4E), neither of which resemble the features obtained for H144*UreE. For H96A/H144*, the changes were less obvious, but a fit to the 1 Cu/dimer spectrum revealed a significant reduction in the A_{xy} value similar to that obtained for H110/H144*. Less dramatic changes were observed for spectra of several other samples including H91A/H144*UreE and Y90F/H144*UreE. Notably, the spectra obtained for C89A, H109A, and D111A variants of H144*UreE do not provide evidence for changes in Cu coordination.

Hyperfine-Shifted ^{1}H NMR. H96A and H110A variants of H144*UreE were examined by ^{1}H NMR in the presence of Ni(II) and Co(II), and these spectra were compared to analogous spectra for H144*UreE (Figure 5). As previously reported, titration of H144*UreE with Ni led to full development of a 62.6 ppm resonance upon addition of the first equivalent of Ni and the further development of resonances at 65.3 and 73.0 ppm with addition of the second equivalent (*21*). The spectrum obtained for H96A/H144*UreE in the presence of a single equivalent of Ni lacked the 63 ppm signal, but exhibited resonances at 65 and 73 ppm. In contrast to the case for H144*UreE, the 65 and 73 ppm resonances of H96A/H144*UreE developed at nearly equal relative intensities in the presence of 1 or 2 equiv of Ni. The spectrum arising from H110A/H144*UreE in the presence of Ni possessed the 63 ppm signal and a weak 65 ppm signal, and lacked any signal at 73 ppm. Titration of the control H144*UreE sample with Co was previously shown to lead to the presence of two resonances with the first metal added, at 63.1 and 76.3 ppm, and a superimposed signal at 76 ppm arising upon addition of the second metal ion (*21*). The spectra for H96A/H144*UreE in the presence of 1 or 2 equiv of Co differed only in signal intensity and lacked the 63 ppm resonance. In contrast, that of the H110A/H144*UreE lacked both of the resonances at 76 ppm.

DISCUSSION

UreE is suggested to facilitate in vivo urease activation; however, this accessory protein is not essential for generating cellular urease activity according to results using mutants containing *ureE* deletions [reported earlier (*17*) and illustrated in Figure 2]. Prior studies had shown that native *K. aerogenes* UreE binds 5−6 Ni/dimer, leading to the reasonable proposal that it functions as a metallochaperone involved in delivery of Ni to the urease apoprotein (*18*). A portion of this Ni binds to the His-rich carboxyl terminus of UreE, but this region of UreE was shown to be irrelevant to its urease activation function by analysis of cells containing the truncated protein, H144*UreE, lacking the His-rich motif [shown earlier (*20*) and confirmed in Figure 2]. Rather, urease activation appears to be associated with two internal Ni-binding sites per dimer that are functional in the truncated

Table 4: Summary of EPR Spectral Parameters for Cu-Substituted H144*UreE Variants[a]

	first equiv of Cu				second equiv of Cu			
UreE	g_z	A_z (G)	$g_{x/y}$	$A_{x/y}$ (G)	g_z	A_z (G)	$g_{x/y}$	$A_{x/y}$ (G)
H144*	2.28	154	2.08/2.05	9/12	2.32	150	2.08/2.06	8/6
C79A/H144*	2.31	138	2.09/2.07	9/12	2.31	139	2.07/2.06	12/10
C89A/H144*	2.27	161	2.07/2.04	10/12	2.32	151	2.08/2.06	8/10
Y90F/H144*	2.27	169	2.08/2.05	11/10	2.32	147	2.08/2.06	7/7
H91A/H144*	2.27	169	2.08/2.05	10/12	2.29	151	2.08/2.05	8/8
H96A/H144*	2.28	156	2.08/2.05	6/6	2.33	145	2.09/2.06	8/7
H109A/H144*	2.28	157	2.07/2.04	10/12	2.31	159	2.08/2.06	8/9
H110A/H144*	2.29	143	2.07/2.05	6/7	–	–	–	–
D111A/H144*	2.28	155	2.07/2.04	11/12	2.31	157	2.09/2.06	8/10
H112A/H144*[b]	2.26	179	2.08/2.05	8/11	–	–	–	–
	2.30	137	2.08/2.05	8/10	–	–	–	–

[a] EPR spectra were collected for H144*UreE variants that were titrated with 1 or 2 equiv of Cu per dimer. Spectra were fitted by POWFIT to obtain the g and A values. Addition of the second equivalent of metal had negligible effects on spectral parameters asssociated with the first site. The estimated error ranges for g_z and $g_{x/y}$ are ±0.01. The error range for A_z is ±10 G. [b] The spectrum for H112A/H144*UreE was comprised of two overlapping species of approximately equal intensity.

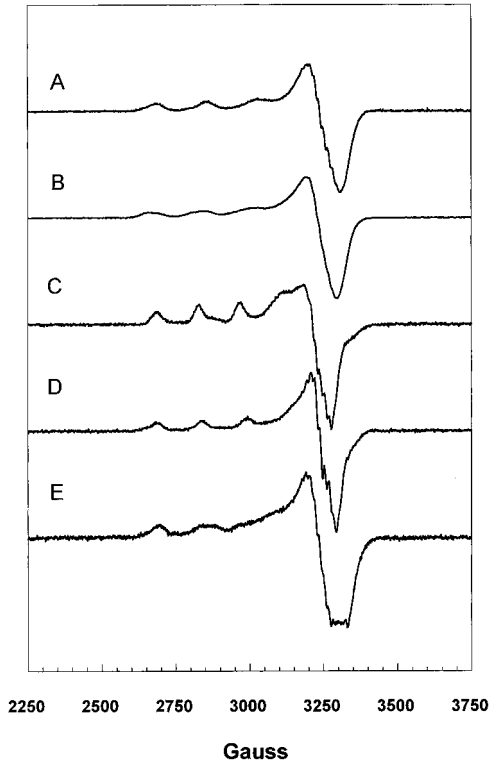

FIGURE 4: Comparison of X-band EPR spectra of the UreE variants to 1Cu− and 2Cu−H144*UreE. Spectra shown are for 1Cu−H144*UreE (A), 2Cu−H144*UreE (B), 1Cu−C79A/H144*UreE (C), 1Cu−H110A/H144*UreE (D), and 1Cu−H112A/H144*UreE (E). Samples (500 μM dimer) were in 20 mM Tris-HCl buffer (pH 7.5) with 100 mM NaCl and 35% glycerol added.

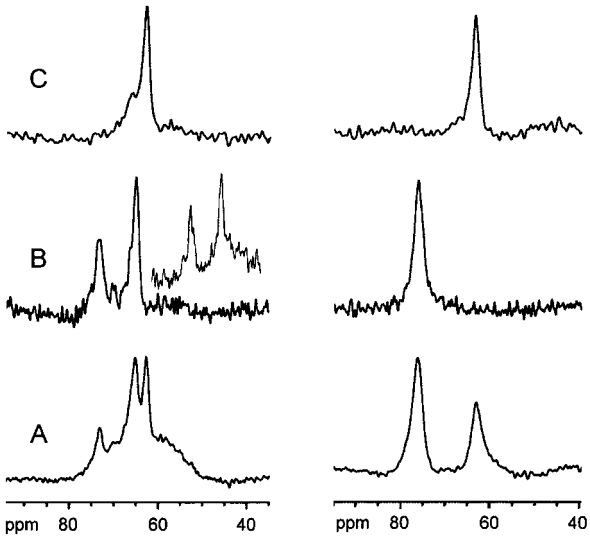

FIGURE 5: Hyperfine-shifted ^{1}H NMR spectra of H144*UreE variants. Spectra shown are for protein samples in the presence of Ni (left) or Co (right). The published spectra for H144*UreE in the presence of 2 equiv of metal are shown (A) for comparison to spectra of H96A/H144*UreE (B) and H110A/H144*UreE (C) prepared in the presence of 2 and 1 equiv, respectively, of the metal ion. The inset (B, left) is the spectrum of H96A/H144*UreE with 1 equiv of Ni, where the intensity of the signal at 73 ppm is normalized to the corresponding signal in the 2 Ni/dimer sample. This signal in (A, left) has been suppressed by the presaturation pulse used for water suppression. The other spectra were acquired with a selective excitation 1-3-3-1 pulse (*30*).

protein (*20*). Although H144*UreE is a homodimer, spectroscopic evidence was reported (*21*) indicating the two internal binding sites are not identical. The studies described here have further probed the internal metal-binding sites of this metallochaperone protein by using a combination of mutagenesis, equilibrium dialysis, and spectroscopic studies. To simplify analyses, we used H144*UreE as our benchmark protein.

Based on our analysis of the properties of H144*UreE and its variants, we have developed a detailed model for metal binding to this accessory protein (Figure 6). The key feature of the model is that two distinct mononuclear metal-binding sites are present per H144*UreE homodimer, with each site symmetrically placed at the dimer interface. The two metallocenters are likely to be close together (e.g., we propose His110 coordinates to one metal while His112 is present as a ligand of the other metal), but the metal sites are not magnetically coupled based on the hyperfine-shifted ^{1}H NMR spectra of Ni- and Co-bound protein (Figure 5) and the EPR signal intensities for Cu-containing samples [(*21*) and Table 4]. The order of metal binding to the sites and the coordination geometries at each site differ depending on the identity of the metal ion. Below, we discuss the detailed interaction of this protein with three metal ions (Ni, Co, and Cu), emphasizing the roles for the individual amino acid residues.

*Ni Binding to H144*UreE.* The two H144*UreE sites involved in Ni binding exhibit partial cooperativity [(*20, 21*)

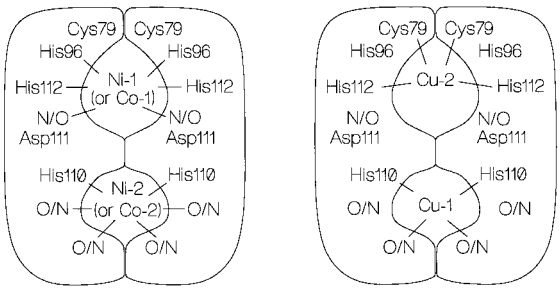

FIGURE 6: Model of the UreE metal-binding sites. Two nonidentical metal-binding sites are proposed to exist at the dimer interface with the metal ions being symmetrically bound at each site. For Ni or Co, the first equivalent of metal ion binds with octahedral coordination to pairs of His96 and His112 ligands from each subunit, as well as two O or N donor atoms. The second equivalent of Ni or Co is bound at a site that includes the pair of His110 residues as well as four additional O/N donors for an overall octahedral coordination. In contrast, the first equivalent of added Cu binds with tetragonal coordination to the H110 pair and two other N/O donors. The second equivalent of Cu binds with tetragonal coordination provided by the H112 pair and at least one Cys79 residue.

and Table 3], thus complicating analysis of the individual sites. Nevertheless, prior X-ray absorption spectroscopy (XAS) studies demonstrate that both Ni ions bind to H144*UreE in octahedral coordination with a mixture of O and N donor atoms, with the first metal ion possessing 3−4 histidine ligands and the second possessing about half this number (reducing the average number of histidine ligands to 2−3) (*21*). The XAS analysis provides no evidence for the presence of a S ligand. Similarly, electronic spectra observed upon addition of Ni to apoprotein provide no indication of a sulfur ligand (i.e., no Cys-to-Ni charge-transfer transition is observed), but do indicate the presence of a d−d transition that is approximately twice as intense in the sample containing two Ni as that containing a single Ni per dimer (*21*). Hyperfine-shifted ^{1}H NMR studies have been reported (*21*) and show that protein containing 1 Ni/dimer exhibits a single predominant paramagnetically shifted resonance at 62.6 ppm, while additional resonances at 65.3 and 73 ppm appear after addition of a second equivalent of Ni. The NMR and XAS methods appear to yield inconsistent results, but as described below these data are compatible within the framework of the model.

We hypothesize that the first equivalent of Ni binds via two symmetric pairs of histidine residues (His96 and His112 from each subunit), as well as two additional unidentified ligands, and that this site is critical for UreE's function in activating urease apoprotein. The presence of four imidazole ligands at the first Ni site is consistent with XAS analysis (*21*). To explain the hyperfine-shifted ^{1}H NMR spectrum of H144*UreE (*21*), we suggest that the 63 ppm resonance be attributed to a single *pair* of His96 residues. Further, we suggest that the second expected resonance due to the *pair* of His112 residues (at 65 ppm) is reduced in intensity because these protons rapidly exchange with solvent. This resonance only appears when the second Ni binds to the protein via the pair of His110 residues, resulting in a decreased rate of exchange for the His112 protons. Evidence that the resonance at 63 ppm arises from His96 is derived from studies with the H96A variant for which this signal is absent (Figure 5). This variant still binds two Ni and exhibits two His ring NH signals assigned to His110 and His112, but consistent with expectations, the affinities for the two separate di-His sites involving His110 and His112 are more similar than for the control protein. In contrast, the H110A variant exhibits the 63 ppm resonance from His96 and a very weak resonance at 65 ppm from His112, but no signal at 73 ppm, consistent with retention of Ni binding at the first site for this protein that binds a single Ni/dimer. The H112A/H144*UreE variant, also capable of binding only a single Ni/dimer, exhibited a shifted d−d transition in its electronic spectrum, compared to the H144*UreE control. The loss of this critical residue at the first binding site eliminates Ni binding to this site and perturbs Ni binding to the second site (altered K_d and UV−visible spectrum). Despite its near-normal binding affinity for Ni, the H96A variant is severely affected in its ability to function in urease activation (Figure 2). Indeed, activation is hindered in this mutant more than for the case where *ureE* is deleted. It is possible that H96A/H144*UreE may sequester Ni within the cell and thus reduce the extent of urease activation. Cells containing either the D111A or the H112A variant of H144*UreE also exhibit significantly reduced levels of urease activity when grown at low nickel ion concentrations, suggesting that they also participate in Ni delivery to urease. Because Asp111 is adjacent to the suspected His112 ligand, it too may coordinate the metal as the N/O donor indicated in Figure 6. Alternatively, Asp111 may participate in a hydrogen-bonding framework associated with this metal-binding site or play some other important role related to metal transfer. To summarize, these results are consistent with His96, Asp111, and His112 being present at the first Ni-binding site in UreE and functioning in urease activation.

We propose that the second equivalent of Ni binds via a symmetric pair of histidine residues (His110 from each subunit), as well as four additional unidentified ligands, and we suggest that this site is not critical to urease activation. According to this model, the average metal coordination environment for protein with two Ni bound per dimer includes three imidazole ligands, consistent with results from XAS analysis (*21*). Binding of the second Ni ion is proposed to lead to cooperative changes at the first Ni-binding site leading to a reduction in the His112 proton exchange rate; thus, the resonances for His110 and His112 (73 and 65 ppm, respectively) simultaneously develop after the second Ni equivalent is added. The three imidazole-derived resonances observed in the NMR spectra (*21*) arise from three symmetric pairs of histidines, or a total of six histidines, which resolves the former confusion between the NMR and XAS results. In agreement with our assignment of the 73 ppm resonance to the His110 pair, the NMR spectrum of H110A/H144*UreE lacks this resonance (Figure 5). Consistent with the lack of importance for this site in urease activation, H110A/H144*UreE, which binds a single Ni ion per dimer, is effective in generating cellular urease activity (Figure 2).

*Co Binding to H144*UreE.* Previous studies had indicated that Co is generally similar to Ni in its binding to H144*UreE (*21*). As is the case with Ni, the electronic absorption spectra show no evidence for a thiolate-to-Co charge-transfer transition, but do show d−d bands that double in intensity as the metal content goes from 1 Co/dimer to 2 Co/dimer. The first Co to bind H144*UreE is associated with two proton NMR resonances (at 63.1 and 76.3 ppm). These two solvent-

exchangeable signals are under fast solvent exchange as their intensities are dramatically decreased when a presaturation pulse on the solvent is applied for spectral acquisition and are fully recovered by use of a selective excitation pulse. The binding of the second metal leads to an increased intensity for the 76 ppm resonance consistent with the presence of an overlapping signal (*21*). Our model retains these aspects of similarity in H144*UreE binding of Co and Ni.

We suggest that the first equivalent of Co binds to the protein via the His96 and His112 pairs, along with two other N/O donors. We attribute the paramagnetically shifted NMR resonances for 1 Co/dimer protein as arising from His96 (63 ppm) and His112 (76 ppm) pairs. Consistent with our assignment, the H96A variant of H144*UreE lacks the 63 ppm signal, while the 76 ppm resonance is retained (Figure 5). In contrast, H110A/H144*UreE exhibits the 63 ppm signal, but possesses no resonance at 76 ppm. We propose that for this variant the empty second site may significantly increase the solvent accessibility to the first site which increases the solvent exchange rate of the His112 ring NH proton so that its signal is abolished. Thus, the spectrum for the Co-containing H110A variant is analogous to that for the 1 Ni/dimer form of H144*UreE in possessing a single paramagnetically shifted NMR resonance.

We hypothesize that the second equivalent of Co binds via the His110 pair and additional unidentified ligands. This binding leads to the development of a third proton NMR resonance (also at 76 ppm) arising from the His110 pair. Consistent with this assignment for the His110 resonance, the NMR signal for H110A/H144*UreE lacks both of the resonances at 76 ppm (Figure 5). The three resonances in the NMR spectrum for H144*UreE thus arise from three symmetric pairs of histidine residues, as suggested for the case of Ni.

*Cu Binding to H144*UreE.* Earlier studies involving EPR and electron spin−echo envelope modulation spectroscopies of H144*UreE had provided evidence that each of its two Cu-binding sites includes two histidine ligands, although the data also revealed that the sites are distinct from each other in their properties (*21*). In contrast to the results for Ni or Co, electronic spectroscopy results of the Cu protein were interpretted as indicating a Cys-to-Cu charge-transfer transition that was associated with binding of the second Cu, not the first (*21*). Resonance Raman spectroscopy was used to confirm the presence of Cys−Cu vibrational frequencies (*21*). In addition, XAS analysis had suggested the presence of two equatorial imidazole ligands for the protein containing a single Cu and for the average site in the 2 Cu/dimer sample. A significantly improved fit was obtained only for the latter sample when a S donor was included as a ligand (*21*). Thus, all of the prior work had suggested that Cu binding was distinct from that observed for Ni or Co; yet, Cu was known to compete with Ni for binding to the protein (*20*).

We propose that the first equivalent of Cu binds to H144*UreE via the His110 pair and 2−4 other O/N donors while the second equivalent of Cu binds via the His112 pair and at least 1 Cys79 residue, with 1−3 other N/O donors. Consistent with this suggestion, the Cys-to-Cu charge-transfer transition is associated with binding of the second metal ion, but is abolished in the C79A and H112A variants. Furthermore, the Cu EPR spectrum for H110A/H144*UreE resembles the second Cu-binding site of H144*UreE (with a greater g_z and smaller A_z and $A_{x/y}$) rather than that typically seen upon addition of the first equivalent (Figure 4). In contrast, the EPR properties associated with the first equivalent of Cu binding to the H96A and D111A variants of H144*UreE were unaffected. Of particular interest, mutations affecting Cys79 and His112 had dramatic effects on the EPR spectral properties associated with the first Cu equivalent. The C79A and H112A variants are likely to bind only a single Cu (unless high concentrations of glycerol are present for the C79A/H144*UreE protein), as further additions of Cu can lead to protein precipitation. This result further establishes a connection between Cys79 and His112 at the same Cu-binding site, i.e., the site associated with the second Cu equivalent. It is not clear why mutations affecting residues that normally bind the second equivalent of Cu also affect EPR parameters measured for the first Cu-binding site, but the proximity of the two sites and the observed partial cooperativity between these sites offer a plausible explanation for how the change is propagated.

UreE Sequence Comparisons. Although it was shown to participate in Ni binding, the His-rich tail found in *K. aerogenes* UreE is not present in UreE sequences from several other microorganisms (Figure 1) and is not required for cellular urease activation (*20*). As illustrated in Figure 1, UreE sequences are poorly conserved among microorganisms that possess a urease gene cluster. In particular, residues homologous to Cys79 (known to participate in Cu binding), His109, and His110 are found in few or no UreE sequences other than that from *K. aerogenes*. Homologues to Cys89, Tyr90, and His91 are more widespread, but not universal, and these UreE residues have been shown to play no important role in urease activation. In contrast, His96 is conserved among all UreE sequences examined, a result that is consistent with its significance in urease activation. Furthermore, Asp111 also is highly conserved and appears to function in urease activation. The most surprisingly aspect of this analysis is that the important Ni-binding residue His112 is not found in most other UreE sequences. It is likely that an alternative O or N donor that is appropriately located near the binding site serves this function in the other species. In summary, the sequence comparisons highlight the conservation of the His96 and Asp111 residues and the lack of conservation among other Ni-binding residues. These findings are consistent with our suggestion that the metal-binding site associated with His 96 is critical for UreE's function as a metallochaperone to facilitate urease activation.

REFERENCES

1. Valentine, J. S., and Gralla, E. B. (1997) *Science 278*, 817−818.
2. Pufahl, R. A., Singer, C. P., Peariso, K. L., Lin, S.-J., Schmidt, P. J., Fahrni, C. J., Culotta, V. C., Penner-Hahn, J. E., and O'Halloran, T. V. O. (1997) *Science 278*, 853−856.
3. Culotta, V. C., Klomp, L. W. J., Strain, J., Casareno, R. L. B., Krems, B., and Gitlin, J. D. (1997) *J. Biol. Chem. 272*, 23469−23472.
4. Srinivasan, C., Posewitz, M. C., George, G. N., and Winge, D. R. (1998) *Biochemistry 37*, 7572−7577.
5. Hausinger, R. P. (1996) in *Mechanisms of Metallocenter Assembly* (Hausinger, R. P., Eichhorn, G. L., and Marzilli, L. G., Eds.) pp 1−18, VCH Publishers, New York.
6. Hausinger, R. P. (1997) *J. Biol. Inorg. Chem. 2*, 279−286.
7. Maier, T., Jacobi, A., Sauter, M., and Böck, A. (1993) *J. Bacteriol. 175*, 630−635.

8. Maier, T., Lottspeich, F., and Böck, A. (1995) *Eur. J. Biochem. 230*, 133−138.
9. Fu, C., Olsen, J. W., and Maier, R. J. (1995) *Proc. Natl. Acad. Sci. U.S.A. 92*, 2333−2337.
10. Rey, L., Imperial, J., Palacios, J.-M., and Ruiz-Argüeso, T. (1994) *J. Bacteriol. 176*, 6066−6073.
11. Olsen, J. W., Fu, C., and Maier, R. J. (1997) *Mol. Microbiol. 24*, 119−128.
12. Kerby, R. L., Ludden, P. W., and Roberts, G. P. (1997) *J. Bacteriol. 179*, 2259−2266.
13. Waugh, R., and Boxer, D. H. (1986) *Biochimie 68*, 157−166.
14. Watt, R. K., and Ludden, P. W. (1998) *J. Biol. Chem. 273*, 10019−10025.
15. Thauer, R. K., and Bonacker, L. G. (1994) *Ciba Found. Symp. 180*, 210−227.
16. Kim, E.-J., Chung, H.-J., Suh, B., Hah, Y. C., and Roe, J.-H. (1998) *Mol. Microbiol. 27*, 187−195.
17. Lee, M. H., Mulrooney, S. B., Renner, M. J., Markowicz, Y., and Hausinger, R. P. (1992) *J. Bacteriol. 174*, 4324−4330.
18. Lee, M. H., Pankratz, H. S., Wang, S., Scott, R. A., Finnegan, M. G., Johnson, M. K., Ippolito, J. A., Christianson, D. W., and Hausinger, R. P. (1993) *Protein Sci. 2*, 1042−1052.
19. Mulrooney, S. B., and Hausinger, R. P. (1990) *J. Bacteriol. 172*, 5837−5843.
20. Brayman, T. G., and Hausinger, R. P. (1996) *J. Bacteriol. 178*, 5410−5416.
21. Colpas, G. J., Brayman, T. G., McCracken, J., Pressler, M. A., Babcock, G. T., Ming, L.-J., Colangelo, C. M., Scott, R. A., and Hausinger, R. P. (1998) *J. Biol. Inorg. Chem. 3*, 150−160.
22. Sambrook, J., Fritsch, E. F., and Maniatis, T. (1989) in *Molecular Cloning: a laboratory manual*, 2nd ed., Cold Spring Harbor Laboratory Press, Cold Spring Harbor, NY.
23. Mulrooney, S. B., Pankratz, H. S., and Hausinger, R. P. (1989) *J. Gen. Microbiol. 135*, 1769−1776.
24. Park, I.-S. (1994) in Ph.D. Thesis, Michigan State University, East Lansing, MI.
25. Weatherburn, M. W. (1967) *Anal. Chem. 39*, 971−974.
26. Lowry, O. H., Rosebrough, N. J., Farr, A. L., and Randall, R. J. (1951) *J. Biol. Chem. 193*, 265−275.
27. Laemmli, U. K. (1970) *Nature 227*, 680−685.
28. Bell, J. E., and Bell, E. T. (1988) in *Proteins and Enzymes*, Prentice-Hall, Inc., New York, NY.
29. P.E.S.T.: *Public EPR Software Tools*, NIEHS, NIH (http://EPR.niehs.nih.gov).
30. Hore, P. J. (1983) *J. Magn. Reson. 54*, 539−542.
31. Jones, B. D., and Mobley, H. L. T. (1989) *J. Bacteriol. 171*, 6414−6422.
32. McMillan, D. J., Mau, M., and Walker, M. J. (1998) *Gene 208*, 243−251.
33. Kaneko, T., Sato, S., Kotani, H., Tanaka, A., Asamizu, E., Nakamura, Y., Miyajima, N., Hirosawa, M., Suguira, M., Sasamoto, S., Kimura, T., Hosouchi, T., Matsuno, A., Muraki, A., Nakazaki, N., Naruo, K., Okumura, S., Shimpo, S., Takeuchi, C., Wada, T., Watanabe, A., Yamada, M., Yasuda, M., and Tabata, S. (1996) *DNA Res. 3*, 109−136.
34. Neyrolles, O., Ferris, S., Behbahani, N., Montagnier, L., and Blanchard, A. (1996) *J. Bacteriol. 178*, 647−655.
35. Chen, Y.-Y., Clancy, K. A., and Burne, R. A. (1996) *Infect. Immun. 64*, 585−592.
36. Maeda, M., Hidaka, M., Nakamura, A., Masaki, H., and Uozumi, T. (1994) *J. Bacteriol. 176*, 432−442.
37. You, J.-H., Song, B.-H., Kim, G.-H., Lee, M.-H., and Kim, S.-D. (1995) *Mol. Cells 5*, 359−369.
38. Cussac, V., Ferrero, R. L., and Labigne, A. (1992) *J. Bacteriol. 174*, 2466−2473.
39. Bossé, J. T., and MacInnes, J. I. (1997) *Infect. Immun. 65*, 4389−4394.
40. Fleischmann, R. D., Adams, M. D., White, O., Clayton, R. A., Kirkness, E. F., Kerlavage, A. R., Bult, C. J., Tomb, J.-F., Dougherty, B. A., Merrick, J. M., McKenney, K., Sutton, G., FitzHugh, W., Feilds, C., Gocayne, J. D., Scott, J., Shirley, R., Liu, L.-I., Glodek, A., Kelley, J. M., Weidman, J. F., Phillips, C. A., Spriggs, T., Hedblom, E., Cotton, M. D., Utterback, T. R., Hanna, M. C., Nguyen, D. T., Saudek, D. M., Brandon, R. C., Fine, L. D., Fritchman, J. L., Fuhrmann, J. L., Geoghagen, N. S. M., Gnehm, C. L., McDonald, L. A., Small, K. V., Fraser, C. M., Smith, H. O., and Venter, J. C. (1995) *Science 269*, 496−512.
41. Riot, B., Berche, P., and Simonet, M. (1997) *Infect. Immun. 65*, 1985−1990.
42. de Koning-Ward, T. F., Ward, A. C., and Robins-Browne, R. M. (1994) *Gene 145*, 25−32.

BI982435T